

SCR-Guided Difficulty-Aware Optimization for Infrared Small Target Detection

Yunus Sevim
Aselsan
Ankara, Turkey
ysevim@aselsan.com

Behçet Uğur Töreysin
Istanbul Technical University
Istanbul, Turkey
toreysin@itu.edu.tr

Abstract

Infrared small target detection remains challenging due to severe background clutter, low contrast, and weak spatial responses where geometric overlap alone is insufficient to characterize detection quality. In this work, we propose REEM (Reweighted Explicit-visibility Enhanced Modulation), a lightweight SCR-guided difficulty-aware optimization framework that incorporates Signal-to-Clutter Ratio (SCR) as a physically meaningful visibility prior during training. Instead of modifying the network architecture or directly optimizing SCR, REEM computes a ground-truth local SCR from the input image and applies a differentiable modulation to the soft-IoU learning signal, emphasizing low-visibility targets while preserving stable optimization and identical inference behavior. REEM is integrated into a U-Net-based MSHNet without introducing additional parameters, architectural modifications, or inference-time overhead. Extensive experiments demonstrate consistent improvements over the baseline, achieving higher IoU and detection probability (P_d) together with substantially reduced false alarms (FA), particularly under challenging low-visibility conditions. These results suggest that SCR-guided difficulty-aware optimization provides an effective and physically grounded complement to conventional overlap-based objectives for infrared small target detection. The code is available at <https://github.com/yall-in-one/Reemm>.

1. Introduction

Infrared small target detection (IRSTD) remains one of the core challenges in infrared search and tracking systems, where reliable perception under adverse sensing conditions is critical [30]. Infrared sensors are increasingly deployed in safety-critical pipelines alongside visible-range cameras, particularly when illumination, weather, or operational constraints degrade the effectiveness of visible-range small object detection methods [12]. IRSTD has broad applications in both civil and military domains, including traffic man-

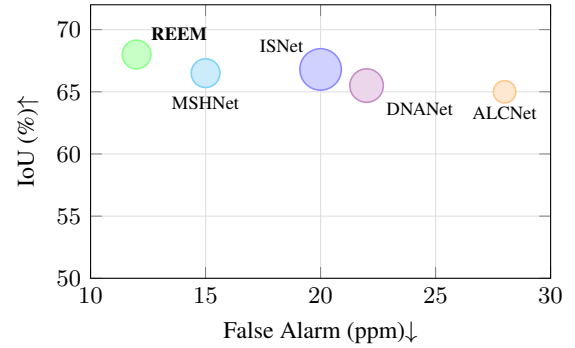


Figure 1. IoU-FA trade-off of representative deep learning-based infrared small-target detectors on IRSTD-1k (test). The x-axis denotes the false alarm rate (FA) in parts per million (ppm), and the y-axis reports IoU (%). Circle area indicates relative model complexity (e.g., parameter count as a proxy). REEM achieves higher IoU at lower false alarm rates compared to prior methods, suggesting a better accuracy-reliability trade-off.

agement [25], maritime surveillance and rescue, navigation, early warning systems, and precise guidance [13, 27]. In contrast to generic object detection [16, 33], which assumes rich appearance cues and sufficient spatial extent, IRSTD must cope with long sensing distances, heavy background clutter, sensor noise, and low signal-to-clutter ratios (SCR), where targets typically span only a few pixels with weak contrast [8, 11, 32].

Infrared small targets under long-range imaging conditions often appear as localized PSF-like intensity responses rather than spatially well-defined objects. Diffraction effects, limited sensor resolution, and atmospheric degradation cause targets to lack stable geometric structures, instead producing compact responses with ambiguous spatial extent and weak shape or texture cues [6]. Consequently, detection performance in IRSTD is often governed more by target-background separability than by precise geometric overlap, which limits the effectiveness of purely appearance-driven learning objectives.

Early IRSTD methods predominantly relied on model-

driven formulations, including filtering-based approaches, local contrast enhancement, and low-rank background modeling [7–9]. While effective in constrained settings, these model-driven approaches rely heavily on handcrafted priors and are sensitive to hyper-parameter selection, often degrading under complex clutter and dynamic backgrounds [21, 23].

With the increasing demand for rapid response and early warning capabilities, single-frame infrared small target detection (SIRST) has attracted growing attention [11], particularly in scenarios where temporal continuity assumptions break down due to fast-moving platforms or targets, making single-frame spatial modeling a more reliable alternative [8]. Recent advances in deep learning, especially encoder–decoder architectures such as U-Net, have enabled data-drivenIRSTD methods that learn discriminative representations directly from annotated data, alleviating the reliance on handcrafted priors [13, 14, 19]. Notable progress has been achieved through specialized network architectures, including dense nested structures, multi-scale feature aggregation, attention mechanisms, contextual modeling, and more recently transformer- and state-space-inspired designs [3, 13, 15, 24, 28].

Despite these architectural advances, most existing deep learning-basedIRSTD methods continue to rely on generic supervision strategies, such as Intersection-over-Union (IoU) loss and Dice loss, originally designed for objects with well-defined spatial extents [20]. However, in regimes where infrared targets exhibit weak visibility, localized intensity responses, or PSF-like characteristics, overlap-based losses may correlate only weakly with detection reliability. Targets with substantially different detectability can produce similar overlap scores, leading to misaligned optimization signals and suboptimal performance, particularly for dim targets embedded in complex background clutter [6, 8].

MSHNet recently showed that meaningful performance gains inIRSTD do not necessarily require more complex architectures [15]. Instead, revisiting the loss function itself can guide feature learning more effectively while keeping the model compact and deployment-friendly. We build on this insight and propose REEM (Reweighted Explicit-visibility Enhanced Modulation), which reweights the training signal according to ground-truth local SCR. Low-visibility targets receive higher gradient emphasis, while high-SCR samples are down-weighted, directly addressing the mismatch between overlap-based losses and true detection difficulty. REEM requires no architectural changes and introduces no inference-time overhead, making it straightforward to apply on top of existingIRSTD frameworks.

2. Related Work

This section reviews three areas directly relevant to the proposed method: single-frameIRSTD approaches, loss function design inIRSTD, and signal-based measures used to characterize target visibility.

2.1. Single-Frame Infrared Small Target Detection

Single-frame infrared small target detection (IRSTD) has been extensively studied due to its practical importance and inherent difficulty. EarlyIRSTD approaches mainly relied on handcrafted priors, including filtering-based methods [7], local-contrast-based techniques [9], and low-rank modeling frameworks [8, 21, 32]. Although effective in constrained scenarios, these methods are highly sensitive to parameter tuning and often exhibit limited robustness under complex and cluttered backgrounds.

With the development of deep learning, convolutional neural network (CNN)-based methods have substantially advanced single-frameIRSTD. Early deep models emphasized background suppression and local contrast enhancement through asymmetric contextual modulation and attention-guided learning [6, 30]. These studies highlighted that suppressing background clutter while preserving weak target responses is essential for reliable infrared perception under challenging imaging conditions.

Subsequent works focused on architectural improvements to maintain small targets in deep representations. Shape-aware supervision was introduced to exploit geometric structure of small targets for improved localization [27]. Dense nested encoder–decoder structures and attention-enhanced U-shaped networks were subsequently introduced to alleviate target disappearance in deep layers and strengthen multi-scale contextual modeling [13, 19].

More recently, transformer-based and hybrid CNN–Transformer architectures have been explored to capture long-range dependencies and global contextual information, which is particularly beneficial for perception tasks beyond the visible spectrum where spatial cues are sparse and ambiguous [2, 24]. In parallel, alternative supervision strategies and efficiency-oriented designs have also been investigated. Adversarial learning frameworks explicitly modeled the trade-off between missed detections and false alarms [22], while single-point supervision and label-evolution schemes reduced annotation cost without sacrificing detection accuracy [23]. Lightweight and real-time detectors were proposed to balance detection performance with computational efficiency [29].

Although these advances have significantly improved detection performance, most existing single-frameIRSTD methods predominantly emphasize architectural design and feature representation. Physically meaningful signal characteristics, which fundamentally govern infrared target detectability, remain relatively underexplored within the

learning objectives of current deep models.

2.2. Geometry-Driven Loss Functions in IRSTD

Loss design plays a central role in deep learning-based infrared small target detection (IRSTD) by shaping how models interpret target-background discrepancies during optimization. Most existing approaches rely on pixel-wise or geometry-driven objectives, including binary cross-entropy (BCE), Dice loss [20], and Intersection-over-Union (IoU), which primarily measure spatial overlap between predictions and ground truth. While effective for general segmentation tasks, such losses remain largely insensitive to variations in target visibility and signal strength, which are critical factors in infrared imagery where targets often appear as faint localized responses.

To improve detection robustness, several studies have explored alternative supervision strategies that remain largely grounded in geometric or appearance-driven paradigms. Adversarial learning frameworks explicitly model the trade-off between missed detections and false alarms through competitive optimization [22], while context- or edge-aware mechanisms aim to enhance boundary sensitivity and local contrast modeling for small targets [6, 27]. Geometry-aware extensions, including Generalized IoU (GIoU) [17] and Complete IoU (CIoU) [31], further improve localization by incorporating geometric constraints such as scale and distance. Similarly, scale- and location-sensitive objectives have been introduced to address ambiguities caused by small target size variations [15]. Despite these advances, these geometry-driven approaches share a common limitation: they optimize spatial correspondence without accounting for visibility-related difficulty, leaving physically meaningful signal characteristics largely unexploited. This limitation motivates the exploration of signal-aware supervision mechanisms that incorporate visibility cues directly into the learning objective, forming the basis of the proposed SCR-guided optimization framework.

2.3. Signal-Based Measures in IRSTD

In infrared imaging, target detectability is fundamentally influenced by the strength of the target signal relative to background clutter and noise. Various signal-based measures have been explored in the IRSTD literature to characterize this relationship.

Signal-to-Noise Ratio (SNR) evaluates the contrast between the target signal and sensor noise and is commonly used to assess imaging quality [14]. While useful in noise-dominated settings, SNR does not capture the effect of structured background clutter, which is the dominant source of difficulty in most infrared scenarios. Contrast-to-Noise Ratio (CNR) jointly considers contrast magnitude and noise variance to evaluate target separability [1]. While widely used in medical and scientific imaging, its application in

IRSTD remains limited, as background clutter rather than noise variance typically governs detection difficulty in infrared scenarios.

Signal-to-Clutter Ratio (SCR) directly measures the relative strength of the target signal against surrounding background structures [8], making it the most informative indicator of target visibility in cluttered scenes. Unlike SNR and CNR, SCR explicitly quantifies target-background separability under realistic infrared conditions, and has been widely adopted to characterize scene difficulty and analyze robustness in low-contrast infrared imagery [30]. This property makes SCR a natural candidate for integration into the learning objective, forming the core motivation of the proposed REEM framework.

Traditional IRSTD pipelines further employ local contrast descriptors and clutter-related statistics to enhance saliency or evaluate background suppression [7–9, 32], yet these measures remain confined to heuristic enhancement rather than end-to-end optimization, underscoring the potential value of signal-aware supervision strategies that better reflect the physical properties of infrared target visibility.

3. Method

This section presents REEM, a lightweight SCR-guided loss reweighting framework for infrared small target detection. We first describe the baseline loss functions used in IRSTD, then introduce the proposed SCR-guided reweighting strategy and its integration into the MSHNet training pipeline.

3.1. Overview of REEM

Infrared small target detection remains challenging due to severe background clutter, low contrast, and weak spatial responses where geometric overlap alone is often insufficient to characterize detection quality. Instead of introducing new network architectures, we propose *REEM*, a lightweight SCR-guided difficulty-aware optimization framework that reshapes the training objective through physically meaningful visibility cues.

The key idea of REEM is to incorporate the Signal-to-Clutter Ratio (SCR) as a visibility prior during training. REEM computes a ground-truth local SCR from the input image and uses it to adaptively reweight the learning signal through a differentiable weighting function, increasing the contribution of low-visibility targets while preserving stable optimization behavior. During training, this SCR-guided reweighting reshapes gradient magnitudes according to target visibility; during inference, the model follows the exact same forward pass as the baseline, introducing no additional parameters or computational overhead.

REEM is implemented on top of the U-Net-based MSHNet framework [15] without modifying the network architecture, prediction head, or inference pipeline, and is readily

applicable to other IRSTD architectures beyond MSHNet.

3.2. Baseline Loss Functions for IRSTD

Most deep learning-based IRSTD methods formulate the task as a pixel-wise segmentation problem and rely on overlap-driven objectives for supervision. Among them, the Intersection-over-Union (IoU) loss is widely used to measure spatial agreement between predicted regions and ground-truth annotations. However, IoU-based supervision is inherently insensitive to variations in target scale and location, which becomes particularly problematic in infrared small target detection where targets often occupy only a few pixels and exhibit weak spatial responses.

To alleviate these limitations, Liu *et al.* [15] introduced the *Scale and Location Sensitive (SLS)* loss, which extends the IoU formulation by incorporating scale discrepancy and center displacement into the optimization objective. The SLS loss decomposes supervision into scale-sensitive and location-sensitive components, encouraging the model to focus on small targets with inaccurate size or localization estimates.

Compared to conventional IoU-based objectives, SLS improves geometric sensitivity without introducing additional network parameters or architectural complexity, making it a strong baseline for IRSTD under small-target regimes.

3.3. SCR-Guided Loss Reweighting

To address the limitations of purely geometry-driven supervision, we introduce a visibility-aware reweighting strategy based on the Signal-to-Clutter Ratio (SCR). Instead of directly optimizing SCR or modifying the network architecture, REEM computes a ground-truth local SCR from the input image and uses it to modulate the learning signal through a differentiable weighting function, increasing the contribution of low-visibility targets while preserving the original geometric supervision.

Formally, let $\mathbf{I} \in \mathbb{R}^{H \times W}$ denote the input infrared image, and let $\mathbf{G} \in \{0, 1\}^{H \times W}$ denote the corresponding ground-truth target mask image of sizes H -by- W pixels. The set of target pixels is defined as

$$\mathcal{T} = \{(x, y) \mid \mathbf{G}(x, y) = 1\}, \quad (1)$$

and the local background region surrounding the target is defined as

$$\mathcal{B} = \{(x, y) \mid (x, y) \in \mathcal{N}(\mathcal{T}) \wedge \mathbf{G}(x, y) = 0\}, \quad (2)$$

where $\mathcal{N}(\mathcal{T})$ denotes a ring-shaped local neighborhood centered at the target bounding box. Specifically, the outer boundary is defined by scaling the bounding box dimensions by a factor of $r_{\text{out}} = 4.0$, and the inner boundary by $r_{\text{in}} = 1.5$. Target pixels are excluded from \mathcal{B} to ensure that

only background clutter statistics are captured. When multiple targets are present in a single image, SCR is computed over the union of all target regions and their corresponding joint bounding box, yielding a single visibility weight per training sample.

The average intensity responses of the target and background regions are computed as

$$\mu_{\mathcal{T}} = \frac{1}{|\mathcal{T}|} \sum_{(x,y) \in \mathcal{T}} \mathbf{I}(x, y), \quad (3)$$

$$\mu_{\mathcal{B}} = \frac{1}{|\mathcal{B}|} \sum_{(x,y) \in \mathcal{B}} \mathbf{I}(x, y), \quad (4)$$

and the background standard deviation is

$$\sigma_{\mathcal{B}} = \sqrt{\frac{1}{|\mathcal{B}|} \sum_{(x,y) \in \mathcal{B}} (\mathbf{I}(x, y) - \mu_{\mathcal{B}})^2}. \quad (5)$$

The local Signal-to-Clutter Ratio (SCR) is then defined as

$$s = \text{SCR} = \frac{|\mu_{\mathcal{T}} - \mu_{\mathcal{B}}|}{\sigma_{\mathcal{B}} + \epsilon}, \quad (6)$$

where s denotes the local signal-to-clutter ratio and ϵ is a small constant for numerical stability.

This formulation follows classical SCR definitions in infrared target detection [8], and is computed locally from the input image using ground-truth supervision, serving as a visibility prior rather than a prediction-dependent objective. Notably, the SLS loss [15] does not incorporate any visibility-aware weighting; all samples contribute equally to the geometric objective regardless of SCR level. REEM therefore introduces a strictly complementary signal: the SCR-guided term $w(\hat{s}) \cdot s\text{IoU}$ modulates only the soft-IoU component, preserving the original optimization landscape while reshaping gradient magnitudes according to target visibility.

Monotonic SCR weighting. To explicitly prioritize low-visibility targets, we define a bounded monotonic weighting function as

$$\hat{s} = \text{clip}(s, 0, s_{\text{max}}), \quad w(\hat{s}) = 1 + \alpha \frac{k}{\hat{s} + k}, \quad (7)$$

where $s_{\text{max}} = 12$ is a saturation threshold that caps extreme high-contrast values to prevent outlier samples from dominating the weighting, $k > 0$ controls the saturation rate, and $\alpha > 0$ determines the maximum upweighting level that separates difficult low-SCR samples from high-visibility ones. The function is strictly decreasing with respect to the clipped SCR:

$$\frac{\partial w}{\partial \hat{s}} = -\alpha \frac{k}{(\hat{s} + k)^2} < 0, \quad (8)$$

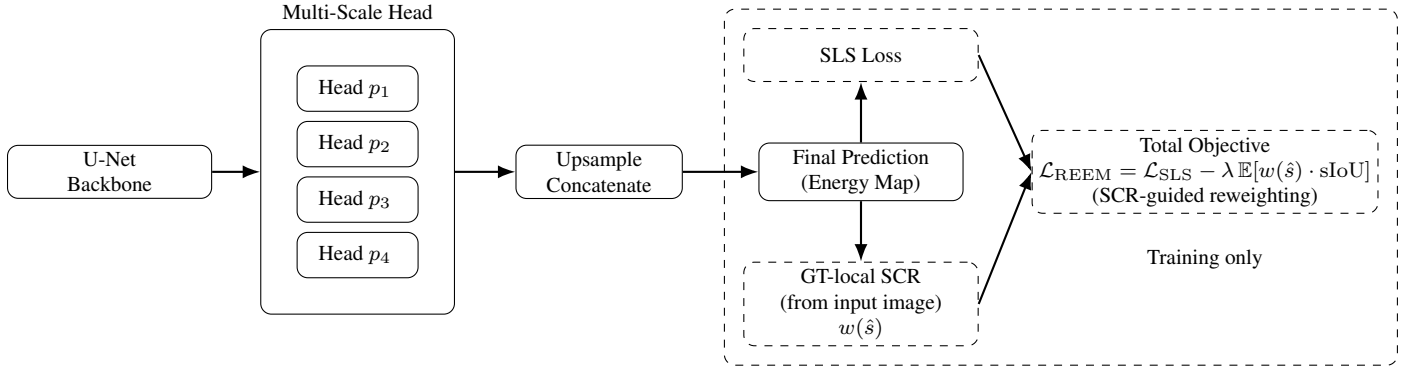


Figure 2. Overview of REEM integrated into MSHNet. REEM preserves the original MSHNet architecture and multi-scale prediction head. During training, the standard SLS loss is applied to the predicted energy map, while a GT-local SCR value is computed from the input image to derive a differentiable weight $w(\hat{s})$, where \hat{s} denotes the clipped SCR defined in Eq. 7, which up-weights the learning signal for low-visibility targets. This SCR-guided weighting modifies only the optimization objective and introduces no additional parameters or inference-time overhead. During inference, REEM follows the standard forward pass of the baseline model, and no SCR evaluation is performed. REEM performs difficulty-aware optimization without altering the model architecture or inference behavior.

and satisfies $w \in [1, 1 + \alpha]$ for $\hat{s} \geq 0$. This formulation ensures that lower-SCR targets receive higher optimization emphasis while maintaining bounded and differentiable gradients. The weighting is applied only during training and introduces no additional inference-time computation.

The total training objective is defined as:

$$\mathcal{L}_{\text{REEM}} = \mathcal{L}_{\text{SLS}} - \lambda \mathbb{E}[w(\hat{s}) \cdot \text{sIoU}], \quad (9)$$

where sIoU denotes the soft Intersection-over-Union component of the SLS loss [15], and $\lambda > 0$ controls the strength of SCR-guided objective modulation.

Unlike heuristic reweighting strategies, $w(\hat{s})$ is computed solely from ground-truth statistics and remains independent of model predictions, introducing no handcrafted decision rules, auxiliary optimization targets, or inference-time overhead.

4. Experimental Analysis

We evaluate REEM on two standard IRSTD benchmarks and compare against both traditional and deep learning-based methods. We also analyze performance across SCR bins to verify that the proposed reweighting strategy specifically benefits low-visibility targets.

4.1. Experimental Setup

Datasets. All experiments are conducted on two widely used infrared small target detection benchmarks, IRSTD-1k [27] and NUDT-SIRST [13], which contain 1,001 and 1,327 infrared images, respectively. In IRSTD-1k, targets occupy a median area of 45 px on 512×512 images; in NUDT-SIRST, the median target area is 40 px on 256×256 images, confirming that both datasets reside firmly in the

small-target regime. We follow the predefined training and testing partitions provided with each dataset to ensure direct comparability with prior IRSTD methods.

Evaluation metrics. We adopt standard evaluation metrics for infrared small target detection, including Intersection-over-Union (IoU), Probability of Detection (Pd), and False Alarm rate (FA). IoU measures pixel-level overlap between predictions and ground truth, Pd evaluates target-level detection accuracy, and FA quantifies the number of false alarm pixels normalized by the image area. Higher IoU and Pd values indicate better detection performance, while lower FA is preferred. Table 1 presents the overall performance comparison on the IRSTD-1k and NUDT-SIRST datasets. Results of existing methods are taken directly from the original MSHNet paper for fair comparison. Unlike prior approaches that rely on increasingly complex network architectures, REEM modifies only the optimization objective and introduces no additional parameters or inference-time overhead.

Evaluation protocol. Unless otherwise stated, we report fixed-threshold results at $\tau = 0.5$. For Pd, we follow the common target-level definition (image-averaged unless specified), and FA is reported in parts-per-million (ppm) normalized by the image area.

Implementation details. REEM is implemented on top of the publicly released MSHNet framework [15] without modifying the original network architecture. The backbone follows the U-Net-based design with a multi-scale prediction head. Input images are resized to 256×256 . Training is performed using the AdaGrad optimizer with an ini-

Table 1. Overall performance comparison on IRSTD-1k and NUDT-SIRST datasets.

Method	Description	IRSTD-1k			NUDT-SIRST		
		IoU \uparrow	Pd \uparrow	FA \downarrow	IoU \uparrow	Pd \uparrow	FA \downarrow
Top-Hat (Morphological) [18]	Filtering	10.06	75.11	1432	20.72	78.41	166.7
Max-Median [7]	Filtering	6.998	65.21	59.73	4.197	58.41	36.89
WSLCM [10]	Local Contrast	3.452	72.44	6619	2.283	56.82	1309
TLLCM [9]	Local Contrast	3.311	77.39	6738	2.176	62.01	1608
IPI [8]	Low Rank	27.92	81.37	16.18	17.76	74.49	41.23
NRAM [26]	Low Rank	15.25	70.68	16.93	6.927	56.40	19.27
RIPT [4]	Low Rank	14.11	77.55	28.31	29.44	91.85	344.3
PSTNN [32]	Low Rank	24.57	71.99	35.26	14.85	66.13	44.17
MSLSTIPT [21]	Low Rank	11.43	79.03	1524	8.342	47.40	888.1
MDvsFA [22]	Deep Learning	37.34	83.71	88.52	35.86	85.22	95.37
ALCNet [5]	Deep Learning	65.68	89.25	27.71	72.89	96.19	30.40
ISNet [27]	Deep Learning	62.88	92.59	27.92	67.86	92.59	34.65
DNANet [13]	Deep Learning	65.35	86.05	21.93	78.28	93.33	15.01
MSHNet [15]	Deep Learning	65.60	93.20	13.51	74.52	95.37	29.00
REEM (ours)	SCR-Aware Reweighting	68.44	93.88	6.30	79.86	97.52	11.21

Note: Higher IoU and Pd indicate better performance, while lower FA is preferred. Results of existing methods are taken directly from the original MSHNet paper, except MSHNet and DNANet which are reproduced using their official implementations under identical experimental settings. All methods are evaluated using a fixed threshold $\tau = 0.5$; Pd and FA are computed with image-averaged normalization (ppm) unless otherwise stated.

tial learning rate of 0.05, following the original MSHNet settings. Unless otherwise stated, all data preprocessing steps, training schedules, and testing pipelines strictly follow the official MSHNet implementation to ensure that performance differences arise solely from the proposed SCR-guided loss reweighting mechanism, rather than architectural or implementation-related factors.

Key observation. REEM primarily improves *reliability* by suppressing clutter-induced responses in low-visibility cases. Under fixed-threshold evaluation ($\tau = 0.5$) on IRSTD-1k, REEM surpasses the baseline MSHNet while preserving the same inference architecture: IoU improves from 65.60% to 68.44%, FA decreases from 13.51 ppm to 6.30 ppm, with a simultaneous gain in Pd (93.20% to 93.88%). On NUDT-SIRST, consistent improvements are observed across all metrics, with IoU increasing from 74.52% to 79.86% and FA decreasing from 29.00 ppm to 11.21 ppm. In SCR-imbalanced datasets such as IRSTD-1k, where approximately 11% of samples fall below $SCR < 2$, standard overlap-driven objectives tend to overfit to easy high-SCR samples. SCR-guided reweighting instead increases the contribution of hard samples, improving target-background separability and reducing false alarms without inference-time heuristics. As summarized in Table 2, performance gains are strongest in low- and mid-SCR regimes: on IRSTD-1k, FA drops from 18.53 ppm to 3.27 ppm in the [1, 2) bin, and from 33.21 ppm to 17.95 ppm in the [2, 4) bin. On NUDT-SIRST, IoU improves by more than 9 points in the $SCR < 1$ regime (67.96% \rightarrow 77.16%). Differences become marginal at $SCR \geq 8$ where detection is already

near saturation, consistent with the expected behavior of the proposed weighting function.

Failure cases. REEM exhibits a consistent limitation in the high-SCR regime ($SCR \geq 8$), where minor degradation in FA is observed on both datasets (IRSTD-1k: 6.36 \rightarrow 6.54 ppm; NUDT-SIRST: 4.44 \rightarrow 9.58 ppm). This behavior stems from the weighting function $w(\hat{s})$, which approaches but never reaches 1 for finite SCR values, resulting in residual gradient updates on already well-detected high-visibility targets. Under a fixed decision threshold, these unnecessary updates slightly shift the decision boundary and can introduce spurious activations on high-contrast background regions. Since REEM is designed to prioritize low-SCR targets, this trade-off is an expected consequence of the proposed objective design rather than a fundamental failure of the method. A straightforward mitigation would be to disable REEM’s reweighting entirely for high-visibility targets; we leave this as future work.

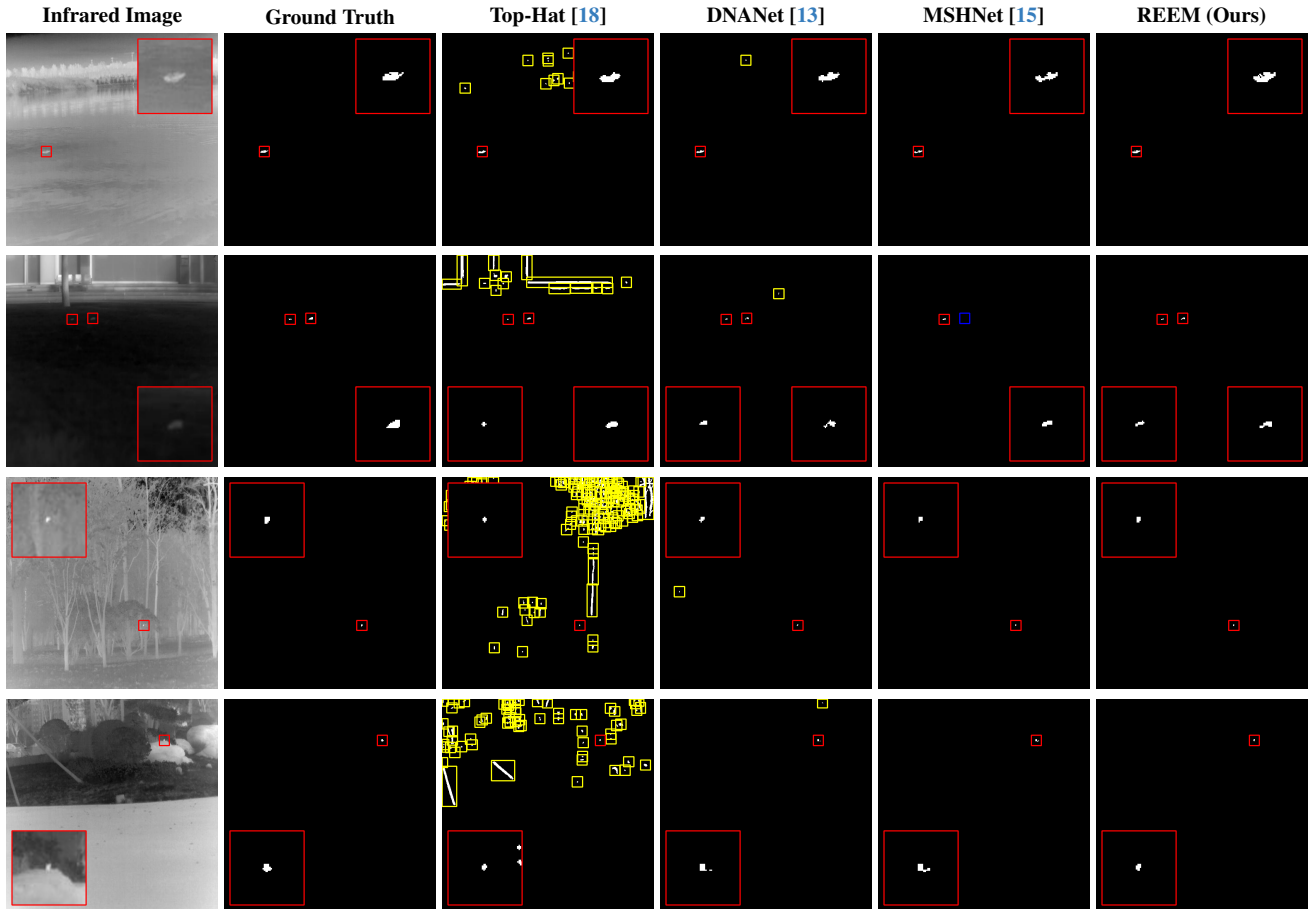


Figure 3. Visual comparison of detection results on representative infrared images. Correct detections, missed targets, and false alarms are indicated by red, blue, and yellow bounding boxes, respectively. Zoomed-in views of target regions are provided in the image corners for clarity. Compared to prior methods, REEM produces cleaner energy responses by suppressing clutter-induced activations while preserving weak small-target signals.

Dataset	SCR	BASE (MSHNet) [15]			REEM		
		IoU \uparrow	Pd \uparrow	FA \downarrow	IoU \uparrow	Pd \uparrow	FA \downarrow
IRSTD-1k	< 1	45.06	78.12	13.35	45.65	84.37	3.81
	[1, 2)	43.87	69.05	18.53	48.08	72.62	3.27
	[2, 4)	59.50	89.22	33.21	61.51	88.73	17.95
	[4, 8)	62.43	96.17	13.51	64.00	96.99	3.00
	≥ 8	63.08	99.60	6.36	62.07	98.41	6.54
NUDT-SIRST	< 1	67.96	87.99	39.04	77.16	94.16	22.19
	[1, 2)	67.53	91.28	40.46	75.14	95.41	11.90
	[2, 4)	75.16	94.55	55.58	79.45	97.58	12.95
	[4, 8)	79.97	97.87	13.53	82.33	98.58	4.65
	≥ 8	86.47	100.00	4.44	89.77	99.42	9.58

Table 2. SCR-binned performance on IRSTD-1k and NUDT-SIRST test sets at a fixed threshold $\tau = 0.5$. SCR is computed using local target-background statistics with edges $\{1, 2, 4, 8\}$. All values are reported as percentages (%) except FA (ppm). Best results within each SCR bin are highlighted in bold.

Inference efficiency. Since REEM modifies only the training objective and introduces no additional computations during inference, its runtime performance remains

identical to the baseline MSHNet in terms of architectural complexity. On an NVIDIA RTX 5080 GPU, the PyTorch implementation achieves approximately **131.8 FPS**

(~ 7.6 ms per frame) for 256×256 inputs. After TensorRT FP16 deployment, throughput increases to **694.9 FPS** (~ 1.44 ms per frame), corresponding to a **5.3 \times speedup**. Importantly, this acceleration does not degrade detection quality: the IoU changes only marginally from 68.49% (PyTorch) to 68.23% (TensorRT), which is within normal numerical variance. These results confirm that the proposed SCR-guided loss reweighting incurs *no inference-time overhead* while remaining fully compatible with high-throughput deployment pipelines.

5. Conclusion

This paper introduced REEM, a physically grounded SCR-guided loss reweighting strategy for infrared small target detection. Rather than designing new network architectures, REEM improves optimization by incorporating signal-to-clutter information as a visibility-aware modulation of the training objective. This formulation enables difficulty-aware learning that emphasizes low-visibility targets while preserving the original model architecture, training pipeline, and inference-time behavior.

Extensive experiments on IRSTD-1k and NUDT-SIRST demonstrate that REEM achieves consistent performance improvements over the MSHNet baseline, with particularly strong gains in low-SCR regimes where conventional overlap-driven supervision often struggles. The results show that integrating physically meaningful signal characteristics into the optimization process provides an effective and lightweight complement to geometry-based loss formulations, improving robustness without introducing additional parameters or computational overhead.

Future work will explore extending SCR-guided optimization to multi-frame and temporal infrared detection settings, investigating signal-aware alternatives to generic difficulty-aware strategies such as focal loss or hard example mining, as well as broader signal-aware supervision strategies for challenging low-contrast vision tasks.

Acknowledgements

Behçet Uğur Töreyn's work was supported in part by the Scientific and Technological Research Council of Türkiye (TUBITAK) with 1515 Frontier Research and Development Laboratories Support Program for the BTS Advanced AI Hub: BTS Autonomous Networks and Data Innovation Laboratory under Project 5239903; in part by the Turk Telekom 6G Research and Development Laboratory under Project 5249902; and in part by the Scientific Research Projects Coordination Department (BAP), Istanbul Technical University under Project ITU-BAP MGA-2024-45372.

References

[1] Jerrold T. Bushberg, J. Anthony Seibert, Edwin M. Leidholdt, and John M. Boone. *The Essential Physics of Medical*

Imaging. Lippincott Williams & Wilkins, 2011. 3

- [2] Gao Chen, Weihua Wang, and Sirui Tan. IRSTFormer: A hierarchical vision transformer for infrared small target detection. *Remote Sensing*, 14(14):3258, 2022. 2
- [3] Tianxiang Chen, Zi Ye, Zhentao Tan, Tao Gong, Yue Wu, Qi Chu, Bin Liu, Nenghai Yu, and Jieping Ye. MiM-ISTD: Mamba-in-mamba for efficient infrared small-target detection. *IEEE Transactions on Geoscience and Remote Sensing*, 62:1–13, 2024. Art. no. 5007613. 2
- [4] Yimian Dai and Yiquan Wu. Reweighted infrared patch-tensor model with both nonlocal and local priors for single-frame small target detection. *IEEE Journal of Selected Topics in Applied Earth Observations and Remote Sensing*, 10(8):3752–3767, 2017. 6
- [5] Yimian Dai, Yiquan Wu, Feng Zhou, and Kobus Barnard. Attentional local contrast networks for infrared small target detection. *IEEE Transactions on Geoscience and Remote Sensing*, 59(11):9813–9824, 2021. 6
- [6] Yimian Dai, Yiquan Wu, Feng Zhou, and Kobus Barnard. Asymmetric contextual modulation for infrared small target detection. In *Proceedings of the IEEE/CVF Winter Conference on Applications of Computer Vision (WACV)*, pages 949–958, 2021. 1, 2, 3
- [7] Suyog D. Deshpande, Meng Hwa Er, Ronda Venkateswarlu, and Philip Chan. Max-mean and max-median filters for detection of small targets. In *Signal and Data Processing of Small Targets*, pages 74–83. SPIE, 1999. 2, 3, 6
- [8] Chenqiang Gao, Deyu Meng, Yi Yang, Yongtao Wang, Xiaofang Zhou, and Alexander G. Hauptmann. Infrared patch-image model for small target detection in a single image. *IEEE Transactions on Image Processing*, 22(12):4996–5009, 2013. 1, 2, 3, 4, 6
- [9] Jinhui Han, Saed Moradi, Iman Faramarzi, Chengyin Liu, Honghui Zhang, and Qian Zhao. A local contrast method for infrared small-target detection utilizing a tri-layer window. *IEEE Geoscience and Remote Sensing Letters*, 17(10):1822–1826, 2019. 2, 3, 6
- [10] Jinhui Han, Saed Moradi, Iman Faramarzi, Honghui Zhang, Qian Zhao, Xiaojian Zhang, and Nan Li. Infrared small target detection based on the weighted strengthened local contrast measure. *IEEE Geoscience and Remote Sensing Letters*, 18(9):1670–1674, 2020. 6
- [11] Sungho Kim. High-speed incoming infrared target detection by fusion of spatial and temporal detectors. *Sensors*, 15(4):7267–7293, 2015. 1, 2
- [12] Onur Can Koyun, Reyhan Kevser Keser, Ibrahim Batuhan Akkaya, and Behçet Uğur Töreyn. Focus-and-detect: A small object detection framework for aerial images. *Signal Processing: Image Communication*, 104:116675, 2022. 1
- [13] Boyang Li, Chao Xiao, Longguang Wang, Yingqian Wang, Zaiping Lin, Miao Li, Wei An, and Yulan Guo. Dense nested attention network for infrared small target detection. *IEEE Transactions on Image Processing*, 32:1745–1758, 2023. 1, 2, 5, 6, 7
- [14] Ming Liu, Hao yuan Du, Yue jin Zhao, Li quan Dong, Mei Hui, and Shawn Xiong Wang. Image small target detection

- based on deep learning with SNR controlled sample generation. In *Current Trends in Computer Science and Mechanical Automation*, pages 211–220. De Gruyter Open Poland, 2017. 2, 3
- [15] Qiankun Liu, Rui Liu, Bolun Zheng, Hongkui Wang, and Ying Fu. Infrared small target detection with scale and location sensitivity. In *Proceedings of the IEEE/CVF Conference on Computer Vision and Pattern Recognition (CVPR)*, pages 17490–17499, 2024. 2, 3, 4, 5, 6, 7
- [16] Joseph Redmon and Ali Farhadi. Yolov3: An incremental improvement. *arXiv preprint arXiv:1804.02767*, 2018. 1
- [17] Hamid Rezatofighi, Nathan Tsoi, JunYoung Gwak, Amir Sadeghian, Ian Reid, and Silvio Savarese. Generalized intersection over union: A metric and a loss for bounding box regression. In *Proceedings of the IEEE/CVF Conference on Computer Vision and Pattern Recognition (CVPR)*, pages 658–666, 2019. 3
- [18] Jean-Francois Rivest and Roger Fortin. Detection of dim targets in digital infrared imagery by morphological image processing. *Optical Engineering*, 35(7):1886–1893, 1996. 6, 7
- [19] Olaf Ronneberger, Philipp Fischer, and Thomas Brox. U-Net: Convolutional networks for biomedical image segmentation. In *Medical Image Computing and Computer-Assisted Intervention (MICCAI)*, pages 234–241. Springer, 2015. 2
- [20] Carole H. Sudre, Wenqi Li, Tom Vercauteren, Sebastien Ourselin, and M. Jorge Cardoso. Generalised dice overlap as a deep learning loss function for highly unbalanced segmentations. In *Deep Learning in Medical Image Analysis and Multimodal Learning for Clinical Decision Support*, pages 240–248. Springer, 2017. 2, 3
- [21] Yang Sun, Jungang Yang, and Wei An. Infrared dim and small target detection via multiple subspace learning and spatial-temporal patch-tensor model. *IEEE Transactions on Geoscience and Remote Sensing*, 59(5):3737–3752, 2020. 2, 6
- [22] Huan Wang, Luping Zhou, and Lei Wang. Miss detection vs. false alarm: Adversarial learning for small target detection in infrared images. In *Proceedings of the IEEE/CVF International Conference on Computer Vision (ICCV)*, pages 8509–8518, 2019. 2, 3, 6
- [23] Xinyi Ying, Li Liu, Yingqian Wang, Ruojing Li, Nuo Chen, Zaiping Lin, Weidong Sheng, and Shilin Zhou. Mapping degeneration meets label evolution: Learning infrared small target detection with single point supervision. In *Proceedings of the IEEE/CVF Conference on Computer Vision and Pattern Recognition*, pages 15528–15538, 2023. 2
- [24] Shuai Yuan, Hanlin Qin, Xiang Yan, Naveed Akhtar, and Ajmal Mian. SCTransNet: Spatial-channel cross transformer network for infrared small target detection. *IEEE Transactions on Geoscience and Remote Sensing*, 62:1–15, 2024. Art. no. 5002615. 2
- [25] Ke Zhang, Shuyan Ni, Dashuang Yan, and Aidi Zhang. Review of dim small target detection algorithms in single-frame infrared images. In *IEEE Advanced Information Management, Communicates, Electronic and Automation Control Conference (IMCEC)*, pages 2115–2120. IEEE, 2021. 1
- [26] Landan Zhang, Lingbing Peng, Tianfang Zhang, Siying Cao, and Zhenming Peng. Infrared small target detection via non-convex rank approximation minimization joint $l_{2,1}$ norm. *Remote Sensing*, 10(11):1821, 2018. 6
- [27] Mingjin Zhang, Rui Zhang, Yuxiang Yang, Haichen Bai, Jing Zhang, and Jie Guo. Isnet: Shape matters for infrared small target detection. In *Proceedings of the IEEE/CVF Conference on Computer Vision and Pattern Recognition*, pages 877–886, 2022. 1, 2, 3, 5, 6
- [28] Mingjin Zhang, Xiaolong Li, Fei Gao, Jie Guo, Xinbo Gao, and Jing Zhang. SAIST: Segment any infrared small target model guided by contrastive language-image pretraining. In *Proceedings of the IEEE/CVF Conference on Computer Vision and Pattern Recognition (CVPR)*, pages 9549–9558, 2025. 2
- [29] Mingxin Zhao, Lei Cheng, Xu Yang, Peng Feng, Liyuan Liu, and Nanjian Wu. TBC-Net: A real-time detector for infrared small target detection using semantic constraint. *arXiv preprint arXiv:2001.05852*, 2019. 2
- [30] Mingjing Zhao, Wei Li, Lu Li, Jin Hu, Pengge Ma, and Ran Tao. Single-frame infrared small-target detection: A survey. *IEEE Geoscience and Remote Sensing Magazine*, 10(2):87–119, 2022. 1, 2, 3
- [31] Zhaohui Zheng, Ping Wang, Wei Liu, Jinze Li, Rongguang Ye, and Dongwei Ren. Distance-IoU loss: Faster and better learning for bounding box regression. In *Proceedings of the AAAI Conference on Artificial Intelligence*, pages 12993–13000, 2020. 3
- [32] Hu Zhu, Haopeng Ni, Shiming Liu, Guoxia Xu, and Lizhen Deng. TNLRS: Target-aware non-local low-rank modeling with saliency filtering regularization for infrared small target detection. *IEEE Transactions on Image Processing*, 29: 9546–9558, 2020. 1, 2, 3, 6
- [33] Zhengxia Zou, Keyan Chen, Zhenwei Shi, Yuhong Guo, and Jieping Ye. Object detection in 20 years: A survey. *Proceedings of the IEEE*, 111(3):257–276, 2023. 1